On the IRS Deployment in Smart Factories Considering Blockage Effects: Collocated or Distributed?

Yixin Zhang, *Member, IEEE*, Saeed R. Khosravirad, *Senior Member, IEEE*,
Xiaoli Chu, *Senior Member, IEEE*, Mikko A. Uusitalo, *Senior Member, IEEE*

***Abstract*—In this article, we study the collocated and distributed deployment of intelligent reflecting surfaces (IRS) for a fixed total number of IRS elements to support enhanced mobile broadband (eMBB) and ultra-reliable low-latency communication (URLLC) services inside a factory. We build a channel model that incorporates the line-of-sight (LoS) probability and power loss of each transmission path, and propose three metrics, namely, the expected received signal-to-noise ratio (SNR), expected finite-blocklength (FB) capacity, and expected outage probability, where the expectation is taken over the probability distributions of interior blockages and channel fading. The expected received SNR and expected FB capacity for extremely high blockage densities are derived in closed-form as functions of the amount and height of IRSs and the density, size, and penetration loss of blockages, which are verified by Monte Carlo simulations. Results show that deploying IRSs vertically higher leads to higher expected received SNR and expected FB capacity. By analysing the average/minimum/maximum of the three metrics versus the number of IRSs, we find that for high blockage densities, both eMBB and URLLC services benefit from distributed deployment; and for low blockage densities, URLLC services benefit from distributed deployment while eMBB services see limited difference between collocated and distributed deployment.**

***Index Terms*—Blockage, deployment, enhanced mobile broadband, finite-blocklength, intelligent reflecting surface, smart factory, ultra-reliable low-latency communications.**

I. Introduction

Industry 4.0 is envisioned to automate or upgrade various industrial processes [1], [2], building on enhanced wireless connectivity offered by the sixth generation (6G) wireless communications technology [3], [4]. The 3rd Generation Partnership Project (3GPP) has defined use cases for the "Factory of the Future", where the wireless performance requirements are mainly specified for two of the 5G service types [3], [5]: enhanced mobile broadband (eMBB) services, such as high definition videos, virtual reality, and augmented reality, which require high data rates and broad bandwidth; and ultra-reliable low-latency communications (URLLC) services, e.g., industrial automation and autonomous driving, which require an end-to-end latency of 0.5-500 ms and a communication service availability ranging from 99.9% to 99.999999%. That results in a striking difference between those two service types, namely, eMBB services use long packets to achieve a high data rate while URLLC services use short packets of a finite blocklength to reduce latency [6], [7]. Accordingly, the evaluation of eMBB and URLLC services in a factory environment relies on the proper choice of performance metrics for them respectively.

Future smart factories will comprise industry equipment, furniture, as well as numerous sensing, computing, and actuating devices, which may become blockages to wireless signal propagation. Multi-hop communication [8], [9], distributed multiple-input multiple-output (D-MIMO) [10], and multi-point coordination [11] schemes have been proposed to facilitate communications in the presence of blockages and clutter. Intelligent reflecting surfaces (IRSs), which are capable of manipulating wireless propagation environments, have emerged as a promising technology to improve link performance even in harsh wireless propagation environments, in a cost-effective and energy-efficient manner [12]–[14]. Both collocated and distributed deployment schemes have been considered for deploying IRSs indoors. In a collocated deployment, all the reflecting elements are arranged into one large IRS; while in a distributed deployment, the reflecting elements are grouped into several small IRSs that can be deployed separately at different locations. For a blockage-ridden smart factory, how IRSs should be deployed (e.g., collocated or distributed) to best support diverse eMBB and URLLC services has not been sufficiently studied.

A. Related Work

Existing works on millimetre wave (mmWave) propagation in factories: The channel characteristics of mmWave signal propagation have been widely studied through measurement campaigns. The authors in [15] provided the results of the path loss and Rician K-factor centred at 28 GHz with a bandwidth of 800 MHz in indoor factory environments. The authors in [16] presented the results of the path gain and the azimuthal angular power distribution at 28 GHz with a receive bandwidth of 20 kHz in a factory. The authors in [17] analysed the path loss and line-of-sight (LoS) probability in both light and heavy industry factories under the candidate frequencies of 28 and 60 GHz for licensed- and unlicensed-band communication,

Yixin Zhang (yixin.zhang@bupt.edu.cn) is with the Key Laboratory of Universal Wireless Communications, Ministry of Education, Beijing University of Posts and Telecommunications, Beijing, China.

Saeed R. Khosravirad (saeed.khosravirad@nokia-bell-labs.com) is with the Nokia Bell Labs, Murray Hill, NJ, USA.

Xiaoli Chu (x.chu@sheffield.ac.uk) is with the Department of Electronic and Electrical Engineering, University of Sheffield, Sheffield, UK.

Mikko A. Uusitalo (mikko.uusitalo@nokia-bell-labs.com) is with the Nokia Bell Labs, Espoo, Finland.

This work is supported in part by the Fundamental Research Funds for the Central Universities under Grant 2023RC18, in part by the National Natural Science Foundation of China (NSFC) under Grant 62321001 and 92267202, in part by the National Key R&D Program of China under Grant 2020YFA0711303, in part by the European Union's Horizon 2020 Research and Innovation Programme under Grant 766231, in part by the Horizon Europe Research and Innovation Program under grant 101086219, in part by EPSRC grant EP/X038971/1, and in part by Guangdong Province Science and Technology Project 2023A0505050127.

respectively, and suggested that mmWave communications in indoor industrial scenarios should take into account the specific geometry of the indoor environment. The authors in [18] noted that the bands 24.25-27.5 GHz and the bands above 52.6 GHz are the candidate bands for Internet-of-things (IoT) applications with high priority, and claimed that the precise models of path loss, LoS probability, root mean-square (RMS) delay spread, and angular spread should consider the antenna height, clutter density, factory volume, and the total surface.

Existing works on distributed cooperative IRSs: In order to overcome the rank deficiency of IRS-assisted wireless networks, multiple IRSs are required to offer spatial multiplexing gains. The authors in [19] found that deploying a large number of finite-size IRSs achieves a higher coverage probability than deploying a small number of large IRSs for a single-input single-output (SISO) system under correlated Rayleigh fading channels. The authors in [20] derived the outage probability of a multi-IRS-assisted SISO system under Rician fading and showed that when the LoS components are stronger than the non-LOS (NLoS) ones, the minimal outage probability, attained through the phase shift alignment between the direct and reflected links, decreases with the number of IRSs and/or the number of elements per IRS. The authors in [21] derived the asymptotic outage probability and average symbol error rate for a distributed IRS aided SISO system under Nakagami-m fading, assuming that the direct and reflected signals are constructively added at the receiver, and unveiled that the achievable diversity order linearly increases with the number of distributed IRSs and the number of elements per IRS. The authors in [22] analysed the ergodic rate of a multiple-input single-output (MISO) system assisted by multiple distributed IRSs considering the impact of channel estimation errors and revealed that the distributed deployment of IRSs is superior to the centralised deployment due to the increased LoS probability of the paths.

Existing works on large-scale IRS deployment: In the large-scale IRS deployment [23]–[26], only one of the multiple randomly deployed IRSs is selected/associated to serve the user equipment (UE). The authors in [23] characterised the spatial throughput of a single-cell multiuser system, and revealed that the system spatial throughput increases when fewer IRSs each with more reflecting elements are deployed, but at the cost of degraded user-rate fairness. The authors in [24] compared the SISO system aided by multiple distributed IRSs or relays, where a user is served by the relay or IRS that leads to the highest received SNR, and concluded that the IRSs outperform relays in terms of outage probability and energy efficiency especially when each IRS is equipped with a large number of IRS elements or the IRSs are more densely deployed. The authors in [25] studied an outdoor cellular network, where the base stations (BSs), IRSs, and blockages are all randomly distributed on a 2D plane, UEs are associated with the BS that offers the lowest average path loss, and a fraction of the blockages are equipped with IRSs. Their results show that a large-scale deployment of IRSs can reduce the blind-spot areas and that coating the blockages at chosen locations with IRSs can reduce the required density of IRSs. The authors in [26] studied the coverage probability of an IRS-assisted LoS mmWave network, and concluded that deploying more small IRSs outperforms deploying fewer large IRSs for small-cell networks with a high user density, e.g., malls and airports.

In smart factories, IRSs are typically deployed on surrounding walls [27], [28]. We note that the existing works on IRS deployment have not sufficiently studied the effects of interior blockages on wireless signal propagation in 3D indoor factory environments. For instance, the widely adopted channel models either assume that the direct link between the BS and the UE is completely blocked (i.e., the blockages are impenetrable [29]) while neglecting the possible residual signal strength passing through the blockages [24]–[26] or assume that both the BS-IRS and IRS-UE links are LoS [20]–[24], which however may not always be the case.

B. Contributions

In this article, we investigate the collocated and distributed IRS deployment strategies in smart factories for a fixed total number of passive reflecting elements, taking into account the effects of interior blockages and different quality-of-service (QoS) requirements of eMBB and URLLC services. The main contributions are summarised as follows:

- We develop a 3D system model for a cubic factory, where a BS is deployed at the centre of the ceiling, a typical UE randomly locates in the blind spot area behind a big tall shelf in the middle of the factory, one or multiple IRSs are deployed on the walls surrounding the blind spot area, and there are interior blockages with random locations and heights modelled following a Poisson point process (PPP) and a uniform distribution, respectively. For the considered typical UE of an arbitrary location in the blind spot area, we derive the LoS probability for each IRS-UE link. This is different from the existing works [20]–[24] that assumed LoS for all IRS-UE links.
- Assuming that each IRS-UE link is either LoS or NLoS independently, we define every distinct combination of LoS/NLoS status of all the IRS-UE links as a blockage case and obtain the probability of occurrence for each blockage case. For an arbitrary blockage case, we derive the expressions of the direct channel from the BS to the typical UE and the indirect channel from the BS via the IRS(s) to the typical UE. This is different from the existing works [24]–[26] where the effects of blockages on the BS-UE channel and BS-IRS-UE channel were not explicitly modelled.
- To facilitate the performance comparison between collocated and distributed IRS deployment strategies, we design three UE location-specific performance metrics, i.e., the expected received SNR, the expected finite-blocklength (FB) capacity, and the expected outage probability, where the expectation is taken over all possible blockage cases and channel fading. The first metric is relevant to eMBB services that require a high received SNR. The second metric is relevant to URLLC services that require a high FB capacity. It can also be applied to eMBB services when the received SNR is relatively high, in which case the expected FB capacity is very

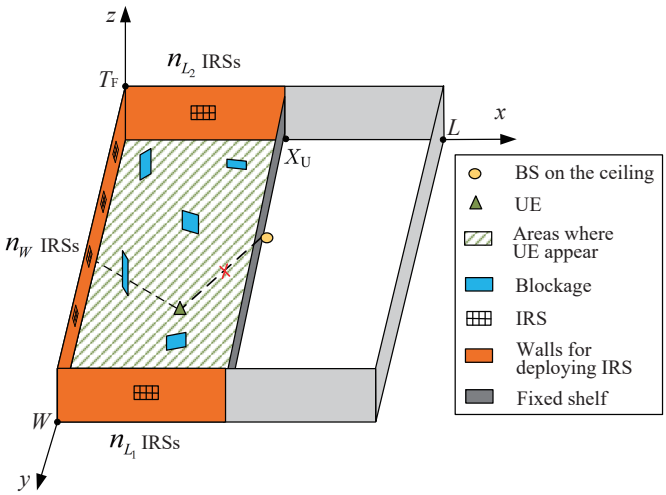

(a)

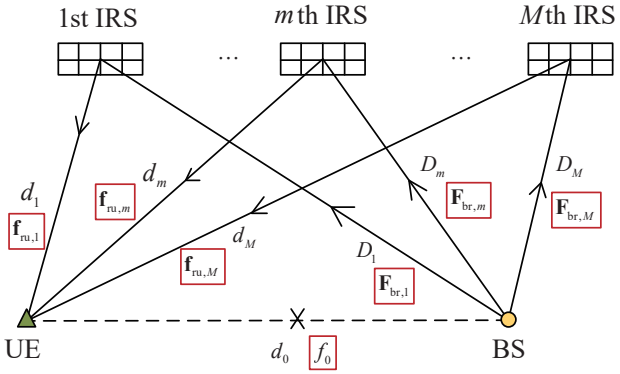

(b)

Fig. 1. System model: (a) A cubic $L \times W \times T_{\mathrm{F}}$ m^3 factory, where the BS is at the centre of the ceiling, blockages are randomly oriented and distributed on the ground, the UE behind the shelf is served with the aid of the IRS(s) on the 3 side walls; (b) The notations and distances of the BS-UE and BS-IRS-UE channels.

close to the expected Shannon capacity. The third metric is relevant to URLLC services that require a low outage probability. This fills in the gap in the existing works on IRS deployment, which have not specifically considered the distinct performance metrics of eMBB and URLLC services.

- The expected received SNR and the expected FB capacity for extremely high blockage densities are derived in closed forms as functions of the number and height of IRSs, the density and size of blockages, and the penetration power loss per blockage. The analytical expressions are verified by Monte Carlo simulations. Our analytical and numerical results show that deploying IRSs higher on the walls results in a higher expected received SNR and a higher expected FB capacity.
- Based on the analytical and simulation results, we obtain the following insights into the IRS deployment in a smart factory: For URLLC services, distributed IRSs outperform collocated IRSs in terms of the minimum expected FB capacity and the maximum expected outage probability across all possible UE locations for both high and low blockage densities. For eMBB services, collocated or distributed IRSs achieve similar values of UE-location averaged expected received SNR and similar values of UE-location averaged expected FB capacity for low blockage densities, but distributed IRSs offer a higher UE-location averaged expected received SNR and a higher UE-location averaged expected FB capacity than collocated IRSs for high blockage densities.

The rest of the article is organised as follows. Section II introduces the system model for IRS-assisted downlink communications in a factory. In Section III, three performance metrics for eMBB and URLLC services are defined and derived. In Section IV, the numerical and simulation results are presented. Finally, Section V concludes this article with guidelines on IRS deployment in smart factories.

II. System Model

A. Factory Environment

As shown in Fig. 1(a), we build a 3D Cartesian coordinate system inside a factory of size $L \times W \times T_{\mathrm{F}}$ m^3, where L, W and T_{F} are the length, width, and ceiling height of the factory, respectively. A BS is located at the centre of the ceiling with the coordinate of $[L/2, W/2, T_{\mathrm{F}}]$. A fixed blocker, e.g., a big tall shelf, whose length and height are close to W and T_{F} respectively, is located in the 2D plane $x = X_{\mathrm{U}}$ parallel to the wall of size $W \times T_{\mathrm{F}}$ and near the BS, i.e., X_{U} is slightly less than $L/2$, thus blocking and causing a power loss of ω to the link between the BS and any UE located behind the shelf. Without loss of generality, we consider a UE[1] at an arbitrary location in the above described blind spot of the BS's coverage area, and denote the UE's coordinate by $[x_{\mathrm{U}}, y_{\mathrm{U}}, T_{\mathrm{U}}]$, where $x_{\mathrm{U}} \in (0, X_{\mathrm{U}})$, $y_{\mathrm{U}} \in (0, W)$, and T_{U} denotes the height of the UE's antenna. For analytical tractability, both the BS and UE are assumed to be equipped with a single antenna.

In order to enhance the wireless communication quality in the blind spot behind the shelf, M cooperative IRSs[2] are deployed on the three walls surrounding the blind spot, i.e., one wall of size $W \times T_{\mathrm{F}}$ on the opposite side of the shelf with respect to the BS and two walls each of size $L/2 \times T_{\mathrm{F}}$ perpendicular to the shelf. The M IRSs are deployed at the same height of h and evenly share a total of N reflective elements, i.e., each IRS has $\frac{N}{M}$ elements that are arranged into an $N_{\mathrm{v}} \times N_{\mathrm{h}}$ planar array with the inter-element spacing of $l = \mu/2$, where μ denotes the wavelength[3]. For simplicity, we assume that $\frac{N}{M}$ is an integer. Specifically, M being 1 corresponds to a collocated IRS deployment, and M being

[1]In a multi-user scenario, orthogonal multiple access of users can be achieved through, e.g., orthogonal frequency division multiple access (OFDMA) [7] or time division multiple access (TDMA) via proper user scheduling [30]. If the considered IRS(s) are associated with at most one user in each OFDMA resource block or TDMA time slot, then the results of this work will still be applicable for individual users in a multi-user scenario.

[2]For analytical tractability, we assume that there is no leakage reflection or interference between any two of the IRSs [31].

[3]For an IRS inter-element spacing of half wavelength, the spatial correlation between any pair of the IRS elements approaches zero [32]. Thus, we assume that the spatial correlation of the IRS-involved channels is negligible.

an integer greater than 1 corresponds to a distributed IRS deployment.

Let n_{L_1} and n_{L_2} denote the number of IRSs deployed on the two walls perpendicular to the shelf, and n_W denote the number of IRSs deployed on the wall parallel to the shelf, subject to $n_{L_1}+n_{L_2}+n_W=M$. Letting $\tau=\frac{W}{X_{\mathrm{U}}}$ denote the aspect ratio of the blind spot area, the number of IRSs evenly deployed on each of the above mentioned three walls is given as follows.

If $\tau \geq 1$, then

$$\begin{aligned} n_{L_1} &= n_{L_2} = \left\lfloor \frac{M}{\tau+2} \right\rfloor, \\ n_W &= M - 2n_{L_1}. \end{aligned} \tag{1}$$

If $\tau < 1$, then

$$\begin{aligned} &n_W = \left\lfloor \frac{\tau M}{2+\tau} \right\rfloor, \\ &n_{L_1} = n_{L_2} = \frac{M-n_W}{2}, \text{if } \ M-n_W \ \text{ is even}, \\ &n_{L_1} = \frac{M-n_W+1}{2}, n_{L_2} = \frac{M-n_W-1}{2}, \text{if } \ M-n_W \ \text{ is odd}, \end{aligned} \tag{2}$$

where $\lfloor \cdot \rfloor$ denotes the floor function.

Accordingly, the deployment location of the mth IRS $\mathbf{q}_m$ is given by

$$\mathbf{q}_m = \begin{cases} \left(0, \frac{m}{n_W+1}W, h\right), m = 1,2,...,n_W, \\ \left(\frac{m-n_W}{2\left(n_{L_1}+1\right)}L, W, h\right), m = n_W+1,...,n_W+n_{L_1}, \\ \left(\frac{m-n_W-n_{L_1}}{2\left(n_{L_2}+1\right)}L, 0, h\right), m = n_W+n_{L_1}+1,...,M. \end{cases} \tag{3}$$

Given the coordinates of the BS, the UE, and the mth IRS for $m=1,2,..,M$, we can calculate the distance from the BS to the UE, the distance from the mth IRS to the UE, and the distance from the BS to the mth IRS, which are denoted by d_0, d_m, and D_m, respectively, as shown in Fig. 1(b).

B. UE-specific Channel Model Considering Blockage Effects

We adopt the stochastic geometry based random blockage model [29], where rectangular screen blockages [33], whose locations are defined by the centres of their bottom lines, are distributed following a PPP with the density of λ_{B} (blockage/m^2) and with their orientations uniformly distributed in $[0,\pi]$. The height of each blockage follows an independent uniform distribution in the range $[T_{\mathrm{U}}, T_{\mathrm{B}}]$, where T_{B} denotes the maximum height of the blockages. We assume $T_{\mathrm{B}} \leq h \leq T_{\mathrm{F}}$ so that the links between the BS and the IRSs are always LoS. The blockages have an identical width of R_{B} m.

The direct channel from the BS to the considered UE is given by

$$f_0 = \sqrt{\beta_0 \omega v^{B_0}} f_{\mathrm{bu}}, \tag{4}$$

where

$$\beta_0 = \frac{G_{\mathrm{T}} G_{\mathrm{R}} \mu^2}{\left(4\pi d_0\right)^2}, \tag{5}$$

denotes the free-space path loss along the the BS-UE link, G_{T} and G_{R} denote the BS transmit and UE receive antenna gain in dBi, respectively, v^{B_0} denotes the total loss caused by the random blockages along the BS-UE link, in which v denotes the attenuation of the signal strength caused by one blockage, and B_0 denotes the number of blockages intersecting the BS-UE link. Since the direct link from the BS to the UE is always blocked due to the fixed shelf, the channel between them sees Raleigh fading, i.e., $f_{\mathrm{bu}} \sim \mathcal{CN}(0,1)$.

For analytical tractability, we assume that the blockages affect each IRS-UE link independently. This assumption holds for most UE locations where the IRS-UE links are independent to one another [29]. Thus, each of the M IRS-UE links can be either LoS or NLoS independently, leading to 2^M different combinations of LoS/NLoS status of the M IRS-UE links. Each of the 2^M combinations is referred to as a blockage case.

A specific blockage case can be represented by a set Ξ, which contains the indices of the LoS IRS-UE links in the corresponding blockage case, where $\Xi \subset \Lambda$, $\Lambda = \{1,2,...,M\}$, and $0 \leq |\Xi| \leq M$. Accordingly, the set $\Lambda \backslash \Xi$ contains the indices of the NLoS IRS-UE links in the blockage case represented by Ξ. Thus, the blockage case Ξ occurs with the probability

$$\zeta_\Xi = \prod_{m \in \Xi} p_m \prod_{w \in \Lambda \backslash \Xi} (1-p_w). \tag{6}$$

Given the random spatial distribution of blockages, the number of blockages intersecting the mth IRS-UE link is a Poisson random variable [29], denoted by B_m. For a specific blockage case Ξ, the number of blockages intersecting the mth IRS-UE link is denoted by $B_{m,\Xi}$, which is a realisation of B_m. Note that $B_{m,\Xi}=0$ only when $m \in \Xi$, while $B_{m,\Xi}$ is a positive integer when $m \in \Lambda \backslash \Xi$.

Lemma 1: Letting $d_{2\mathrm{D},0}$ and $d_{2\mathrm{D},m}$ denote the horizontal distances in the XOY plane of the BS-UE link and the mth IRS-UE link, respectively, the expected number of blockages intersecting the BS-UE link and the mth IRS-UE link are, respectively, given by

$$E(B_0) = \frac{(T_{\mathrm{B}} - T_{\mathrm{U}})}{(T_{\mathrm{F}} - T_{\mathrm{U}})} \frac{\lambda_{\mathrm{B}} R_{\mathrm{B}} d_{2\mathrm{D},0}}{\pi}, \tag{7}$$

$$E(B_m) = \frac{(T_{\mathrm{B}} - T_{\mathrm{U}})}{(h - T_{\mathrm{U}})} \frac{\lambda_{\mathrm{B}} R_{\mathrm{B}} d_{2\mathrm{D},m}}{\pi}, m = 1,2,..,M, \tag{8}$$

where $E(\cdot)$ denotes the expectation; and the LoS probability of the mth IRS-UE link is given by

$$p_m = \exp(-E(B_m)), m = 1,2,..,M. \tag{9}$$

Proof: See Appendix A. ■

For the blockage case Ξ, the indirect channel from the BS via the M IRSs to the considered UE is given by

$$f_\Xi = \sum_{m=1}^{M} \sqrt{\beta_m v^{B_{m,\Xi}}} \mathbf{f}_{\mathrm{ru},m} \Theta_m \mathbf{F}_{\mathrm{br},m}, \tag{10}$$

where

$$\beta_m = \frac{G_{\mathrm{T}} G_{\mathrm{R}} \mu^2}{(4\pi)^3} \left(\frac{l}{D_m d_m} \right)^2 \cos^2(\varphi_m), \forall m = 1, 2, ..., M, \tag{11}$$

denotes the free-space path loss along the mth IRS-UE link [34], in which φ_m denotes the incident angle with respect to the mth IRS; $v^{B_{m,\Xi}}$ denotes the total loss caused by the blockages along the mth IRS-UE link under blockage case Ξ; $\Theta_m \in \mathbb{C}^{N/M \times N/M}$ denotes the phase shift matrix of the mth IRS and is given by

$$\Theta_m = \mathrm{diag}[e^{j\theta_{m,1}}, e^{j\theta_{m,2}}, ..., e^{j\theta_{m,N/M}}], \tag{12}$$

where $\theta_{m,n}$ denotes the phase shift at the nth element of the mth IRS, $m = 1, 2, ..., M$, $n = 1, 2, ..., N/M$, and $\mathrm{diag}[\cdot]$ denotes the diagonal matrix.

The LoS channel between the BS and the mth IRS, $\mathbf{F}_{\mathrm{br},m} \in \mathbb{C}^{N_{\mathrm{h}} N_{\mathrm{v}} \times 1}$, is given by [35]

$$\mathbf{F}_{\mathrm{br},m} = \frac{1}{N_{\mathrm{h}} N_{\mathrm{v}}} \mathrm{vec}^T \left(\mathbf{W} \left(\delta_{\mathrm{br},m}^{(h)}, \delta_{\mathrm{br},m}^{(v)}, N_{\mathrm{h}}, N_{\mathrm{v}} \right) \right), \tag{13}$$

where $\delta_{\mathrm{br},m}^{(h)}$ and $\delta_{\mathrm{br},m}^{(v)}$ denote the horizontal and vertical angle of arrival (AOA) from the BS to the mth IRS, respectively, and $(\cdot)^T$ denotes the transpose, $\mathrm{vec}(\cdot)$ denotes row vectorisation of a matrix, the $(n_{\mathrm{h}}, n_{\mathrm{v}})$th element of $\mathbf{W}\left(\delta^{(h)}, \delta^{(v)}, N_{\mathrm{h}}, N_{\mathrm{v}}\right)$ is given by

$$\begin{aligned} &\left[\mathbf{W} \left(\delta^{(h)}, \delta^{(v)}, N_{\mathrm{h}}, N_{\mathrm{v}} \right) \right]_{(n_{\mathrm{h}}, n_{\mathrm{v}})} \\ &= \exp\left(j \frac{2\pi}{\lambda} l \sin\delta^{(v)} \left((n_{\mathrm{h}} - 1) \cos\delta^{(h)} + (n_{\mathrm{v}} - 1) \sin\delta^{(h)} \right) \right), \end{aligned} \tag{14}$$

for $n_{\mathrm{h}} = 1, 2, ..., N_{\mathrm{h}}$, $n_{\mathrm{v}} = 1, 2, ..., N_{\mathrm{v}}$.

The channel between the mth IRS and the UE, $\mathbf{f}_{\mathrm{ru},m} \in \mathbb{C}^{1 \times N/M}$, is assumed to follow Rician fading, i.e.,

$$\mathbf{f}_{\mathrm{ru},m} = \sqrt{\frac{K_{\mathrm{ru},m}}{1 + K_{\mathrm{ru},m}}} \bar{\mathbf{f}}_{\mathrm{ru},m} + \sqrt{\frac{1}{1 + K_{\mathrm{ru},m}}} \tilde{\mathbf{f}}_{\mathrm{ru},m}, \tag{15}$$

where $K_{\mathrm{ru},m}$ denotes the Rician factor and is given by [15]

$$K_{\mathrm{ru},m} = \begin{cases} 7.34 - 0.046 d_m \ (\mathrm{dB}), \text{if } m \in \Xi, \\ 0, \text{if } m \in \Lambda \backslash \Xi, \end{cases} \tag{16}$$

$\bar{\mathbf{f}}_{\mathrm{ru},m}$ and $\tilde{\mathbf{f}}_{\mathrm{ru},m}$ denote the LoS and NLoS components, respectively,

$$\bar{\mathbf{f}}_{\mathrm{ru},m} = \frac{1}{N_{\mathrm{h}} N_{\mathrm{v}}} \mathrm{vec} \left(\mathbf{W} \left(\delta_{\mathrm{ru},m}^{(h)}, \delta_{\mathrm{ru},m}^{(v)}, N_{\mathrm{h}}, N_{\mathrm{v}} \right) \right), \tag{17}$$

in which $\delta_{\mathrm{ru},m}^{(h)}$ and $\delta_{\mathrm{ru},m}^{(v)}$ denote the horizontal and vertical angle of departure (AOD) from the mth IRS to the UE, respectively, each element of $\tilde{\mathbf{f}}_{\mathrm{ru},m}$ is assumed to be i.i.d. following Gaussian distribution with a zero mean and unit variance.

In order to enable constructive received signal combining at the UE, the optimal phase shift matrices of the M IRSs given in (12) are configured based on f_{bu}, $\mathbf{f}_{\mathrm{ru},m}$, and $\mathbf{F}_{\mathrm{br},m}$ [21] as follows:

$$\begin{aligned} \theta_{m,n} = &\arg(f_{\mathrm{bu}}) - \arg(f_{\mathrm{ru},m,n}) - \arg(F_{\mathrm{br},m,n}), \\ &m = 1, 2, ..., M, n = 1, 2, ..., N/M, \end{aligned} \tag{18}$$

where $f_{\mathrm{ru},m,n}$ and $F_{\mathrm{br},m,n}$ denote the nth element of $\mathbf{f}_{\mathrm{ru},m}$ and $\mathbf{F}_{\mathrm{br},m}$, respectively.

Accordingly, the signal received at the UE under blockage case Ξ is given by

$$r = f_0 t + f_\Xi t + n, \tag{19}$$

where r, t, n denote the received signal, the transmitted signal with the transmission power of P_{T} (dBm), and the additive white Gaussian noise with the power of P_{W}, respectively, f_0 and f_Ξ are given in (4) and (10), respectively. Given the noise figure of σ (dB) and the bandwidth of Z (MHz), P_{W} is given by $P_{\mathrm{W}} = -174 + \sigma + 10\log_{10} Z$ (dBm) [36]. Then, the transmit SNR ρ is calculated via $P_{\mathrm{T}} - P_{\mathrm{W}}$ in dB and via $10^{(P_{\mathrm{T}} - P_{\mathrm{W}})/10}$ in linear scale.

Hence, the received SNR under blockage case Ξ is given by

$$\begin{aligned} \gamma_\Xi &= \rho |f_0 + f_\Xi|^2 \\ &= \rho \left(\sqrt{\beta_0 \omega v^{B_0}} |f_{\mathrm{bu}}| + \sum_{m=1}^{M} \sqrt{\beta_m v^{B_{m,\Xi}}} \sum_{n=1}^{N/M} |f_{\mathrm{ru},m,n}| \right)^2. \end{aligned} \tag{20}$$

For URLLC services in smart factories, typical packets are very short in order to meet the stringent latency requirement [3], and the channel capacity is evaluated using the FB channel capacity [7]. Under blockage case Ξ, the FB channel capacity in bit/s/Hz is given by [27]

$$C_\Xi^{\mathrm{FB}} = \log_2(1 + \gamma_\Xi) - \sqrt{\frac{1}{S} - \frac{1}{S(1 + \gamma_\Xi)^2}} \frac{Q^{-1}(\varepsilon)}{\ln 2}, \tag{21}$$

where S denotes the blocklength in nat, ε denotes the decoding error probability, and Q^{-1} denotes the inverse Q function.

The outage probability under blockage case Ξ is given by

$$\begin{aligned} P_\Xi &= \Pr\left(\log_2\left(1 + \rho |f_0 + f_\Xi|^2 \right) < R \right) \\ &= \Pr\left(|f_0 + f_\Xi|^2 < \frac{2^R - 1}{\rho} \right), \end{aligned} \tag{22}$$

where R denotes the capacity threshold in bit/s/Hz.

III. Performance Metrics

In this section, we define three new UE location-specific performance metrics, i.e., the expected received SNR, the expected FB capacity, and the expected outage probability, which can be used to compare the collocated and distributed IRS deployment schemes in smart factories. The first two metrics are relevant to eMBB services, while the last two metrics are relevant to URLLC services. For extremely high blockage densities, the expected received SNR and the expected FB capacity are derived in closed forms.

A. Expected Received SNR

Based on the probability ζ_Ξ of blockage case Ξ in (6) and the received SNR under Ξ in (20), the expected received SNR for all possible Ξ at a specific UE location is defined as

$$\gamma = \sum_{\Xi} \zeta_\Xi E(\gamma_\Xi). \tag{23}$$

Theorem 1: In extremely high blockage density scenarios (i.e., λ_b is large but finite), γ approaches $E(\gamma_{\varnothing})$, where $\gamma_{\varnothing} = \gamma_{\Xi}$ for Ξ being a null set corresponding to the high-density blockage case that has no LoS IRS-UE link at all, and $E(\gamma_{\varnothing})$ is given as a function of M, h, λ_{B}, R_{B}, and v in (24).

Proof: See Appendix B. ∎

Remark 1: In extremely high blockage density scenarios, since $E(\gamma_{\varnothing})$ monotonically decreases with λ_{B} and R_{B}, while monotonically increases with v, the expected received SNR at any UE location decreases with the density of blockages, the size of each blockage, and the loss caused by each blockage.

Remark 2: In a given blockage scenario of an extremely high density and for a given number of IRSs, since $E(\gamma_{\varnothing})$ monotonically increases with h, deploying the IRSs at a higher position results in a larger expected received SNR at any UE location.

Remark 3: In a given blockage scenario of an extremely high density and for a given number and deployment height of IRSs, the expected received SNR varies with the UE location.

B. Expected FB Capacity

Based on (6) and the FB capacity under Ξ in (21), the expected FB capacity for all possible Ξ at a specific UE location is defined as

$$C^{\mathrm{FB}} = \sum_{\Xi} \zeta_{\Xi} E\left(C_{\Xi}^{\mathrm{FB}}\right). \tag{25}$$

Note that when the received SNR is relatively high, the expected FB capacity can also be used to evaluate the performance for eMBB services, which are usually evaluated using the Shannon capacity. This is because as γ_{Ξ} increases, the difference between the FB capacity in (21) and the Shannon capacity, $\log_2(1+\gamma_{\Xi})$, becomes a small constant value determined by the decoding error probability and the blocklength [37, eq. (1)].

Theorem 2: For an extremely high blockage density (i.e., λ_b is large but finite) and low transmit SNR, C^{FB} approaches $E\left(C_{\varnothing}^{\mathrm{FB}}\right)$, and is upper bounded by

$$\bar{C} = \log_2\left(1+E\left(\gamma_{\varnothing}\right)\right) - \sqrt{\frac{1}{S} - \frac{1}{S(1+E\left(\gamma_{\varnothing}\right))^2}}\frac{Q^{-1}(\varepsilon)}{\ln 2}, \tag{26}$$

where $C_{\varnothing}^{\mathrm{FB}} = C_{\Xi}^{\mathrm{FB}}$ for Ξ being a null set, and $E(\gamma_{\varnothing})$ is given in (23).

Proof: Since C_{Ξ}^{FB} is a concave function of γ_{Ξ}, based on the Jensen's inequality and (21), for $\Xi = \varnothing$, we have

$$E\left(C_{\varnothing}^{\mathrm{FB}}\right) \le \log_2\left(1+E\left(\gamma_{\varnothing}\right)\right) - \sqrt{\frac{1}{S} - \frac{1}{S(1+E\left(\gamma_{\varnothing}\right))^2}}\frac{Q^{-1}(\varepsilon)}{\ln 2}. \tag{27}$$

The upper bound given on the right-hand side of (27) becomes tighter for a lower transmit SNR ρ. This is because as ρ decreases, $C_{\varnothing}^{\mathrm{FB}}$ approaches a linear function of $\gamma_{\varnothing}$, leading to a diminishing gap between $E\left(C_{\varnothing}^{\mathrm{FB}}\right)$ and its upper bound $\bar{C}$. ∎

C. Expected Outage Probability

Based on (6) and the outage probability under Ξ in (22), the expected outage probability for all possible Ξ at a specific UE location is defined as

$$P = \sum_{\Xi} \zeta_{\Xi} P_{\Xi}. \tag{28}$$

It is difficult to obtain a closed-form expression of P because the probability density function (PDF) of the sum product of the power loss caused by a random number of blockages, i.e., v^{B_0} and v^{B_m}, and the channel fading coefficients, i.e., $|f_{\mathrm{bu}}|$ and $\sum_{n=1}^{N/M} |f_{\mathrm{ru},m,n}|$, is unknown and analytically intractable. But fortunately, it is easy to calculate (28) numerically, hence P can be used to quickly evaluate the performance of various collocated and distributed IRS deployment.

IV. Numerical Results

In this section, we consider the service area of 19.5×50 m^2 behind the shelf in a cubic factory of $40 \times 50 \times 5$ m^3, where we will investigate the collocated and distributed IRS deployment schemes by taking the number of IRSs being 1, 4, 8, 12, 16 as examples. The corresponding deployment configurations are shown in Table I. The area of interest is sampled at 2 m resolution, resulting in 250 sampling UE locations over the service area. For every UE location, the Monte Carlo simulation results of the three metrics, i.e., the expected received SNR, the expected FB capacity, and the expected outage probability, are calculated averaged over 1E7 realisations, comprised of 2500 random blockage drops times

$$E\left(\gamma_{\varnothing}\right) = \frac{\rho G_{\mathrm{T}} G_{\mathrm{R}} \mu^2}{16\pi^2} \times \left(\begin{array}{l} \frac{\omega}{d_0^2} \exp\left(\frac{-(T_{\mathrm{B}}-T_{\mathrm{U}})\lambda_{\mathrm{B}} R_{\mathrm{B}} d_{\mathrm{2D},0}(1-v)}{(T_{\mathrm{F}}-T_{\mathrm{U}})\pi}\right) \\ + \frac{Nl\sqrt{\pi\omega}}{4Md_0} \exp\left(\frac{-(T_{\mathrm{B}}-T_{\mathrm{U}})\lambda_{\mathrm{B}} R_{\mathrm{B}} d_{\mathrm{2D},0}\left(1-\sqrt{v}\right)}{(T_{\mathrm{F}}-T_{\mathrm{U}})\pi}\right) \sum_{m=1}^{M} \frac{\cos\varphi_m}{D_m d_m} \exp\left(\frac{-(T_{\mathrm{B}}-T_{\mathrm{U}})\lambda_{\mathrm{B}} R_{\mathrm{B}} d_{\mathrm{2D},m}\left(1-\sqrt{v}\right)}{(h-T_{\mathrm{U}})\pi}\right) \\ + \frac{N^2 l^2}{16M^2} \sum_{m=1}^{M} \sum_{p=1, p\neq m}^{M} \frac{\cos\varphi_m}{D_m d_m} \frac{\cos\varphi_p}{D_p d_p} \exp\left(\frac{-(T_{\mathrm{B}}-T_{\mathrm{U}})\lambda_{\mathrm{B}} R_{\mathrm{B}} (d_{\mathrm{2D},m}+d_{\mathrm{2D},p})\left(1-\sqrt{v}\right)}{(h-T_{\mathrm{U}})\pi}\right) \\ + \frac{Nl^2}{4\pi M}\left(1-\frac{\pi}{4}+\frac{N}{M}\right) \sum_{m=1}^{M} \left(\frac{\cos\varphi_m}{D_m d_m}\right)^2 \exp\left(\frac{-(T_{\mathrm{B}}-T_{\mathrm{U}})\lambda_{\mathrm{B}} R_{\mathrm{B}} d_{\mathrm{2D},m}(1-v)}{(h-T_{\mathrm{U}})\pi}\right) \end{array} \right) \tag{24}$$

TABLE I: IRS deployment schemes

M	1	4	8	12	16
n_{L_1} or n_{L_2}	0	0	1	2	3
n_W	1	4	6	8	10
N_{h}	32	16	12	10	10
N_{v}	30	15	10	8	6

TABLE II: Main simulation assumptions

Parameter name	**Parameter value**
Frequency (GHz)	28
Factory width W (m)	50
Factory length L (m)	40
Factory height T_{F} (m)	5
Inter IRS element spacing $l = \mu/2$ (m)	0.0054
The x coordinate of the fixed shelf X_{U} (m)	19.5
Number of total IRS elements N	960
The power loss of the fixed shelf ω (dB)	20
The power loss of a random blockage υ (dB) [38]	20
The width of a random blockage R_{B} (m) [33]	2.5
The maximum height of the blockages T_{B} (m) [33]	1.7
UE height T_{U} (m)	0.5
Transmit power P_{T} (dBm)	22
Noise figure σ (dB)	9
Bandwidth Z (MHz)	400
Transmit antenna gain G_{T} (dBi)	24
Receive antenna gain G_{R} (dBi)	10
Capacity threshold R (bit/s/Hz)	0.1
Blocklength S (nat)	200
Decoding error rate ϵ	1E-9

4000 channel fading coefficients. Other parameters used in the simulations are given in Table II. Note that for URLLC services, low expected outage probability and high expected FB capacity are desired, while for eMBB services, high expected received SNR and high expected FB capacity are desired.

Fig. 2 shows the CDF of the expected received SNR for λ_{B} being 0.05, 0.2, 1 blockage/m^2, where $M = 8$, $P_{\mathrm{T}} = 30$ dBm, and $h = 4$ m. As the blockage density increases, the CDF lines of the expected received SNRs move left, leading to lower received SNRs at a relatively low percentile, which confirms *Remark 1*. This is intuitive because the UE located further away from the BS and/or IRSs would be affected more significantly by the blockage density. Besides, the analytical results in (24) become tighter to the simulation results when the blockage density gets higher, which validates *Theorem 1*.

Fig. 3 depicts the CDF of the expected FB capacity for P_{T} being 30 dBm, 0 dBm, and -30 dBm, where $M = 12$, $\lambda_{\mathrm{B}} = 1$ blockage/m^2 and $h = 4$ m. We can see that, the expected FB capacity decreases when the transmit power is reduced. Meanwhile, by reducing the transmit power, the gap between the simulation and analytical results calculated using (26) gets smaller, which verifies *Theorem 2*.

Figs. 4(a)-(c) present the expected received SNR for M being 1, 8 and 16, respectively, where $\lambda_{\mathrm{B}} = 1$ blockage/m^2, $P_{\mathrm{T}} = 30$ dBm, and $h = 4$ m. We observe that the fairness of the expected received SNRs over the service area is substantially enhanced. The expected received SNRs of the UE located close to the corners or some walls of the room can be improved as the number of IRSs increases. When the number of IRSs increases from 1 to 8 and 16, the UE at the worst location that receives minimum expected received SNRs

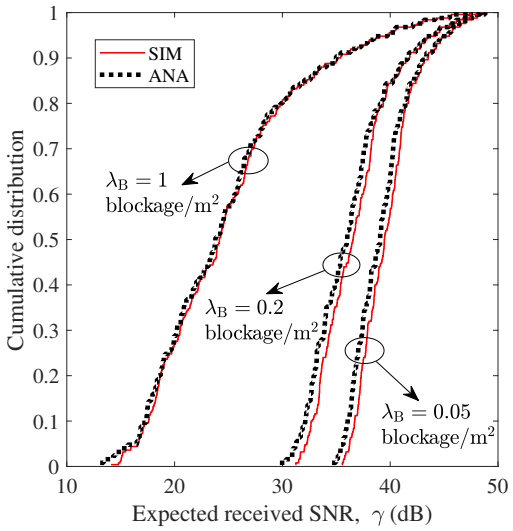

Fig. 2. The CDF of the expected received SNRs γ in (23) at 250 sampling UE locations over the service area of 19.5×50 m^2 for λ_{B} being 0.05, 0.2, 1 blockage/m^2, where $M = 8$, $P_{\mathrm{T}} = 30$ dBm, and $h = 4$ m. Lines represent the simulation values while markers represent the analytical values calculated using (24).

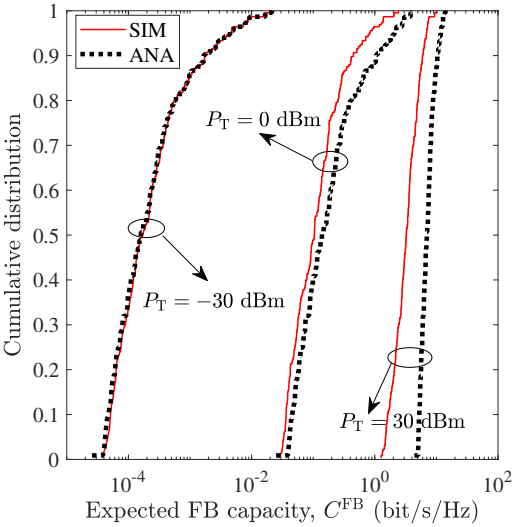

Fig. 3. The CDF of the expected FB capacities C^{FB} in (25) at 250 sampling UE locations over the service area of 19.5×50 m^2 for P_{T} being -30, 0, 30 dBm, where $M = 12$, $\lambda_{\mathrm{B}} = 1$ blockage/m^2, and $h = 4$ m. Lines represent the simulation values while markers represent the analytical values calculated using (26).

can receive 7.5 and 10.7 more dB, respectively. However, comparing the 1-IRS deployment and 16-IRS deployment, the UEs close to the BS or the IRS(s) have to make some compromise, as evidenced by the expected received SNR of the UE located at (1, 25, 0.5) and (20, 25, 0.5) decreased by 18.4 dB and 0.05 dB, respectively. Note that most of the analytical results calculated by (24) match well with the simulation results, while the gap between analytical and simulation results gets larger as the number of IRSs increases, especially for the UE locations near the 3 surrounding walls. That is because the number of blockages intersecting each

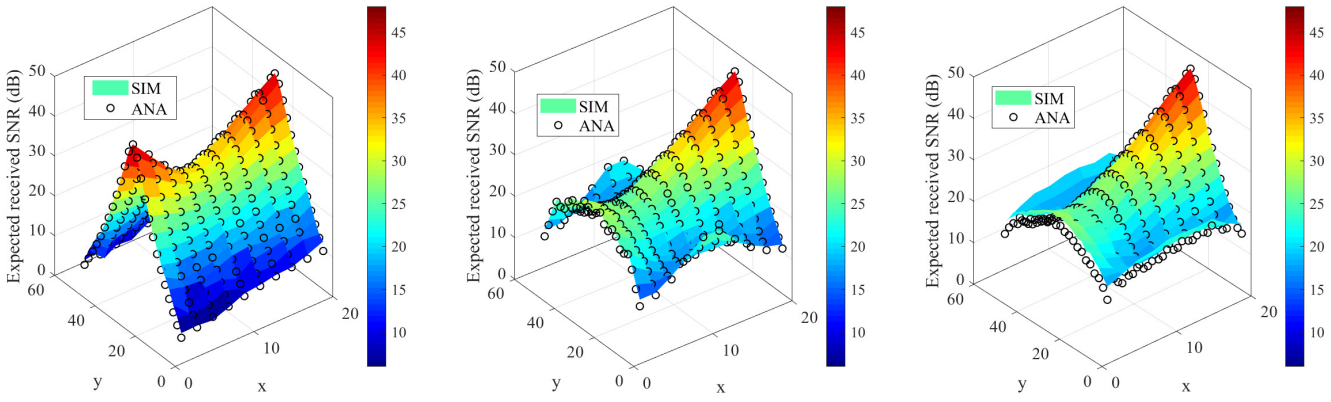

(a) $M = 1$ (b) $M = 8$ (c) $M = 16$

Fig. 4. The expected received SNRs at 250 sampling UE locations over the service area of 19.5×50 m^2 for (a) $M = 1$, (b) $M = 8$, (c) $M = 16$, where $\lambda_{\mathrm{B}} = 1$ blockage/m^2, $P_{\mathrm{T}} = 30$ dBm, and $h = 4$ m. Surfaces represent the simulation values while markers represent the analytical values obtained using (24).

IRS-UE link is not strictly independent to each other as the UE gets closer to the IRSs and the space between adjacent IRSs becomes smaller. Nonetheless, the analytical results calculated by (24) show the same trend as the simulated results of the expected received SNRs at all UE locations, and hence can be used to quickly evaluate and analyse the IRS deployment in smart factories [29].

In Fig. 5, the CDF of the expected FB capacity for M being 1, 8, 16 under $\lambda_{\mathrm{B}} = 0.2$ or 0.05 blockage/m^2 scenarios are presented, where $P_{\mathrm{T}} = 30$ dBm, and $h = 4$ m. The no-IRS deployment schemes are also plotted as benchmarks. For a same blockage density, at relatively low percentiles, the expected FB capacity increases with the number of IRSs. The CDFs of the expected FB capacity converge for large numbers of IRSs, e.g., $M = 8$ and $M = 16$. This indicates that the expected FB capacity stops further increasing when the number of IRSs is sufficiently large, especially at relatively high percentiles. For instance, comparing the 16-IRS scheme and the 1-IRS scheme with the no-IRS scheme, respectively, the minimum capacities are raised by 75% and 147%, when $\lambda_{\mathrm{B}} = 0.2$ blockage/m^2. Under the same comparison, for $\lambda_{\mathrm{B}} = 0.05$ blockage/m^2 scenarios, the minimum capacities are upgraded by 38% and 46%, respectively. With the increase of blockage density, the expected FB capacity decreases.

Figs. 6(a)-(b) illustrate the CDF of the expected outage probability for M being 1, 4, 8, 12, 16, in $\lambda_{\mathrm{B}} = 0.2$ blockage/m^2 and $\lambda_{\mathrm{B}} = 0.05$ blockage/m^2 scenarios, respectively, with the no-IRS schemes plotted as benchmarks, where $P_{\mathrm{T}} = 30$ dBm, and $h = 4$ m. For both considered blockage densities, compared with the no-IRS deployment scheme, the expected outage probability can be depressed by at least four orders of magnitude with the aid of IRS deployment. When deploying distributed IRSs, the expected outage probability can be further reduced by one or two orders of magnitude, but the reduction slows down when the number of IRSs exceeds 12. Comparing Fig. 6(a) with Fig. 6(b), we can see that the minimum required number of IRSs for achieving the same expected outage probability increases with the blockage density.

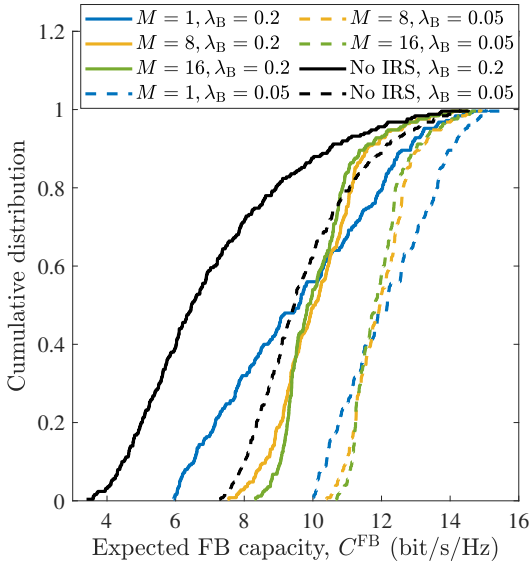

Fig. 5. The CDF of the expected FB capacities C^{FB} in (25) at 250 sampling UE locations over the service area of 19.5×50 m^2 for M being 1, 8, 16, where λ_{B} is either 0.05 or 0.2 blockage/m^2, and $h = 4$ m.

To summarise, in terms of the expected received SNR and expected FB capacity, leveraging more distributed IRSs to assist wireless communications will improve the fairness among all UE locations by sacrificing the superior performance of a small group of UEs enabled by collocated IRSs. In addition, the expected outage probability can also be suppressed by using distributed IRSs.

A. The impact of M and h for practical high blockage density scenario (i.e., $\lambda_B = 0.2$ blockage/m^2)

In Fig. 7, the mean/minimum/maximum values of the expected received SNR, the expected FB capacity, and the expected outage probability among 250 sampling UE locations

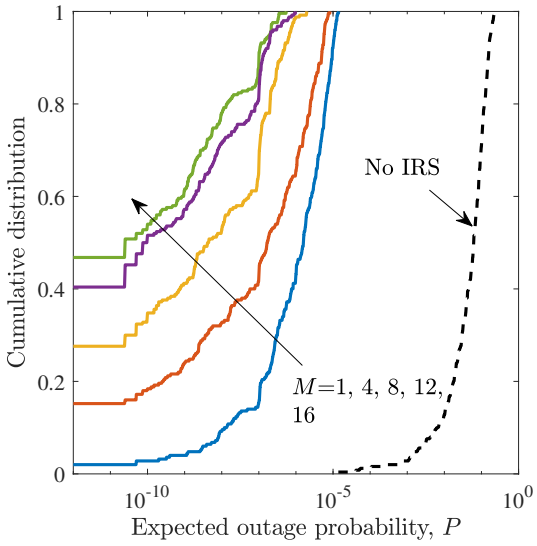

(a) $\lambda_B = 0.2$ blockage/m^2

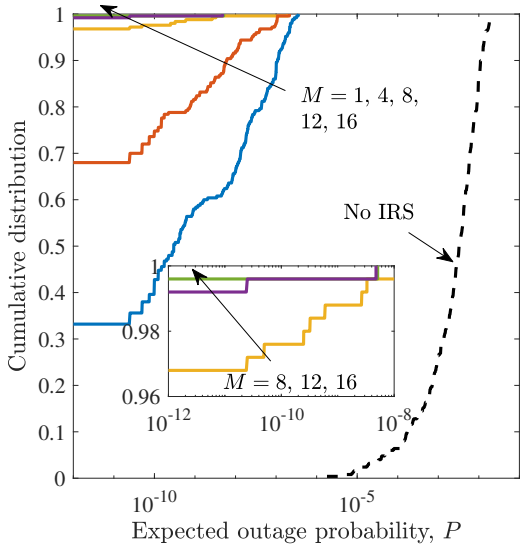

(b) $\lambda_B = 0.05$ blockage/m^2

Fig. 6. The CDF of the expected outage probability P in (28) at 250 sampling UE locations over the service area of 19.5×50 m^2 for M being 1, 4, 8, 12, 16 under (a) $\lambda_B = 0.2$ blockage/m^2, (b) $\lambda_B = 0.05$ blockage/m^2 scenarios, where $P_T = 30$ dBm, and $h = 4$ m.

versus the number of IRSs for different IRS height of 2, 3, 4 m are shown, where $\lambda_B = 0.2$ blockage/m^2, $P_T = 30$ dBm.

Generally, under any number of IRSs deployed, raising the height of IRSs will always enhance the average/minimum expected received SNR and average/minimum expected FB capacity, and reduce the average/maximum expected outage probability, which demonstrates that higher deployment of IRS ensures greater availability of the IRS-UE links, as shown in *Remark 2*.

With regards to the expected received SNR, we can tell from in Fig. 7(a) and Fig. 7(d) that its average decreases with the number of IRSs, however, its minimum increases with the number of IRSs. Compared with 16-IRS deployment, the 1-IRS deployment trades a 1.05 dB decrease in average performance for a 1.14 dB improvement in minimum performance when the IRS is deployed at 4 m high, and trades a 0.35 dB decline in average performance for a 3.98 dB enhancement in minimum performance when the IRS is deployed at 2 m high. That is to say, even if there is limit in the height of the IRS deployment, decentralising the IRS elements into more units benefits the fairness of received SNRs among different UE locations.

Fig. 7(b) and Fig. 7(e) show the average and minimum expected FB capacity with respect to the number of IRSs, respectively. We can see that both the mean and minimum expected FB capacity increase with a declining growth speed when more distributed IRSs are deployed. When enlarging the IRS units from 1 to 16, the minimum expected FB capacity can be enhanced nearly 71%, 52% and 38%, respectively, for the IRS height of 2, 3, 4 m. Although the average performance converges to a constant when the number of IRSs exceeds 8, the minimum performance at the worst UE location can still achieve nearly 1 more bit/s/Hz when continue increasing the number of IRSs to 16.

Fig. 7(c) and Fig. 7(f) illustrate the average and maximum expected outage probability versus the number of IRSs, respectively, where all the curves show a downward trend against the number of IRSs. Comparing the 16-IRS scheme with the 1-IRS scheme, the average expected outage probability can be reduced by a factor of 110, 70, and 35, for the IRS deployment height of 4 m, 3 m, and 2 m, respectively, while the maximum expected outage probability can be reduced by a factor of 26, 25, 17, for the IRS deployment height of 4 m, 3 m, and 2 m, respectively. Obviously, using distributed IRS deployment schemes will pull up the probability of meeting the capacity requirement, allowing the wireless system to support more demanding use cases. It is noteworthy that deploying IRSs higher on the chosen walls make the reduction in expected outage probability more pronounced.

Overall, in order to combat the heavy blockage effects in high blockage density scenarios, distributing the fixed number of IRS elements into a larger amount of IRSs and deploying them higher on the chosen walls is lucrative for URLLC services. On the contrary, for eMBB services, it is not advisable to deploy a large number of distributed IRSs, e.g., increasing the number of IRSs beyond 8 offers trivial gains.

B. The impact of M and h for practical low blockage density scenario (i.e., $\lambda_B = 0.05$ blockage/m^2)

In Fig. 8, the mean/minimum/maximum values of the expected received SNR, the expected FB capacity, and the expected outage probability among 250 sampling UE locations versus the number of IRSs for different IRS height of 2, 3, 4 m are depicted, where $\lambda_B = 0.05$ blockage/m^2, $P_T = 30$ dBm.

As shown in Fig. 8(a) and Fig. 8(b), the average expected received SNR and the averaged expected FB capacity basically decrease with the number of IRSs, except the values for the average expected FB capacity for the IRS height of 2 m remain

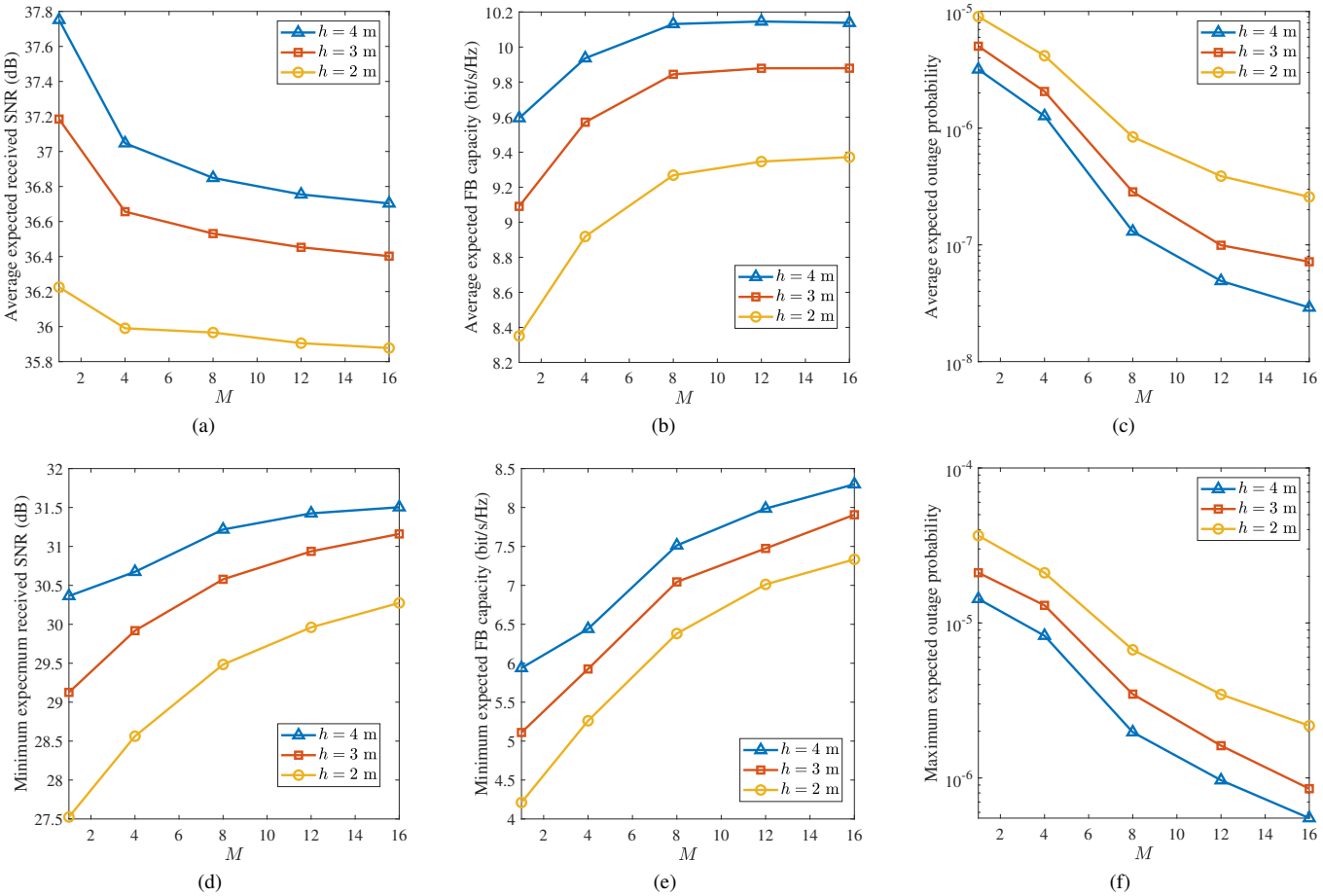

Fig. 7. The mean/minimum/maximum values of the expected received SNR, expected FB capacity, and expected outage probability among 250 sampling UE locations versus the number of IRSs for different IRS height of 2, 3, 4 m, where $\lambda_{\mathrm{B}} = 0.2$ blockage/m^2, $P_{\mathrm{T}} = 30$ dBm.

almost unchanged. As shown in Fig. 8(d) and Fig. 8(e), the minimum expected received SNR and the minimum expected FB capacity show slight upward trends when the number of IRSs is enlarged.

As mentioned before, the minimum performance can be improved by sacrificing a little average performance. To illustrate, adding up the number of IRSs at 2 m high from 1 to 16 causes 0.89 dB decrease in averaged expected received SNR and 0.03 bit/s/Hz increase in averaged expected FB capacity, while leading to a 1.13 dB increase in minimum expected received SNR and a 1.14 bit/s/Hz increase in minimum expected FB capacity. For the IRS height being 4 m, deploying 16 IRSs instead of 1 IRS compromises the average expected received SNR of 1.14 dB and the average expected FB capacity of 0.24 bit/s/Hz, but at the same time brings about a 0.46 dB increase in minimum expected received SNR and a 0.65 bit/s/Hz increase in minimum expected FB capacity. Moreover, we observe that the improvement in the minimum expected SNR and minimum expected capacity becomes more limited when the IRSs are lifted from 3 m to 4 m high than from 2 m to 3 m, especially for the number of IRSs being 12 and 16.

In Fig. 8(c) and Fig. 8(f), the average and maximum expected outage probability are generally getting lower when the amount of IRS grows from 1 to 16. The IRS deployment at 2 m and 3 m height show similar performance in the average and maximum expected outage probability for the amount of IRS being 1, 4, 8, 12, 16. In addition, for the number of IRSs being 1, 4, and 8, raising the IRS(s) to 4 m height does not change much the average/maximum expected outage probability as compared to the IRS deployment at 2 m or 3 m height, nonetheless, when the number of IRSs goes up from 8 to 12 or 16, the averaged/maximum expected outage probability will be significantly declined by more than 40 times.

Therefore, for practical low blockage densities, there is not much difference between the collocated and distributed IRS deployment schemes for eMBB services. Nevertheless, for URLLC services, it is preferable to use more than 8 distributed IRSs deployed at 4 m high on the chosen walls to suppress the maximum expected outage probability. Moreover, it may not be very cost-effective to adopt more than 12 distributed IRSs for user fairness, due to the marginal gains in minimum expected FB capacity and maximum expected outage probability.

V. Conclusions

In this article, we have constructed a new channel model for analysing collocated or distributed IRS deployment in a cubic

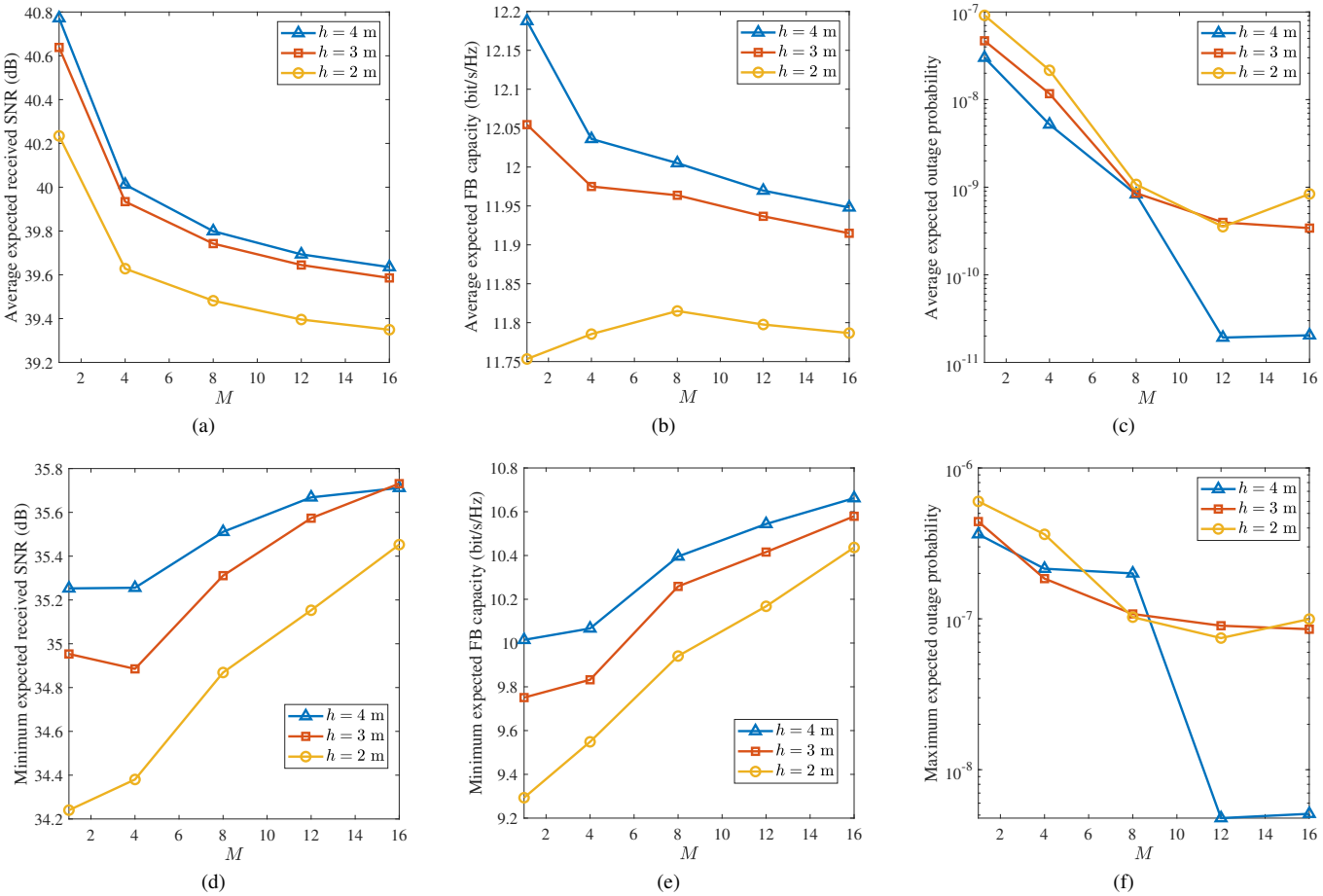

Fig. 8. The mean/minimum/maximum values of the expected received SNR, expected FB capacity, and expected outage probability among 250 sampling UE locations versus the number of IRSs for different IRS height of 2, 3, 4 m, where $\lambda_{\mathrm{B}} = 0.05$ blockage/m^2, $P_{\mathrm{T}} = 30$ dBm.

factory, taking the effects of interior blockages into account. Targeting eMBB and URLLC services in smart factories, we have proposed three performance metrics, i.e., the expected received SNR, the expected FB capacity, and the expected outage probability, where the expectation is taken over all possible blockage cases and channel fading realisations. For extremely high blockage densities, we have derived the closed-form expressions of the expected received SNR and expected FB capacity. The analytical expressions are validated by Monte Carlo simulations.

Based on our analytical and simulation results, we obtain the following insights into the deployment of multiple IRSs for supporting eMBB and URLLC services in smart factories.

- For high blockage densities, distributing a fixed total number of IRS elements into more IRSs and deploying them higher on the chosen walls will lead to a higher expected received SNR and a higher expected FB capacity, thus benefiting both eMBB and URLLC services.
- For low blockage densities, eMBB services can be well supported by either collocated or distributed IRSs; while for URLLC services, deploying distributed IRSs higher on the chosen walls can effectively suppress the expected outage probability.
- In terms of the expected received SNR and expected FB capacity, leveraging more distributed IRSs will improve the fairness among all UE locations.
- The expected outage probability can be suppressed by using distributed IRSs. The minimum required number of IRSs for achieving the same expected outage probability increases with the blockage density.
- There exists an optimal number of distributed IRSs, beyond which the marginal gains in the expected received SNR, expected FB capacity, and expected outage probability become negligible.
- The expected received SNR or expected FB capacity or expected outage probability for the UEs located further away from the BS and/or IRSs would be affected more significantly by the blockage density, compared with the UEs located near the BS and/or IRSs.

Potential future directions of this work are multi-fold: 1) the analysis of IRS deployment for supporting eMBB and URLLC services under multi-user interference in multi-user smart factory scenarios; 2) the design of IRS deployment while considering potential leakage reflections and interference between distributed IRSs; 3) the deployment of IRSs while considering the IRS inter-element spacing and the spatial correlation of the IRS-involved channels.

APPENDIX A

Considering the height of a random blockage, the number of blockages that intersects the BS-UE link and the mth IRS-UE link are Poisson random variables, whose expectations can be respectively derived by [29, Theorem 3],

$$E(B_0) = \eta_1 E(B_{2\mathrm{D},0}), \tag{29}$$

$$E(B_m) = \eta_2 E(B_{2\mathrm{D},m}), \tag{30}$$

where $B_{2\mathrm{D},0}$ and $B_{2\mathrm{D},m}$ denote the number of blockages that intersects the projection lines in the XOY plane of the BS-UE link and the mth IRS-UE link, respectively, η_1 denotes the conditional probability of blocking the BS-UE link given its projection line in the XOY plane is intersected by a blockage, and η_2 denotes the conditional probability of blocking the IRS-UE link given its projection line in the XOY plane is intersected by a blockage.

Particulary, $B_{2\mathrm{D},0}$ and $B_{2\mathrm{D},m}$ are also Poisson random variables, whose expectations are given by [29, Theorem 1]

$$E(B_{2\mathrm{D},0}) = \frac{2\lambda_{\mathrm{B}} R_{\mathrm{B}} d_{2\mathrm{D},0}}{\pi}, \tag{31}$$

$$E(B_{2\mathrm{D},m}) = \frac{2\lambda_{\mathrm{B}} R_{\mathrm{B}} d_{2\mathrm{D},m}}{\pi}. \tag{32}$$

Since the height of the blockage is not greater than T_{B}, the BS-UE link will not be blocked when a blockage is horizontally separated from the UE beyond S_1 m in the XOY plane, where

$$S_1 = \frac{T_{\mathrm{B}} - T_{\mathrm{U}}}{T_{\mathrm{F}} - T_{\mathrm{U}}} d_{2\mathrm{D},0}. \tag{33}$$

Then

$$T_{s_1} = \frac{(T_{\mathrm{F}} - T_{\mathrm{U}})\, s_1}{d_{2\mathrm{D},0}} + T_{\mathrm{U}} \tag{34}$$

represents the minimum height of a blockage intersecting the BS-UE link when the blockage is horizontally separated from the UE by s_1 m in the XOY plane, where $0 \le s_1 \le S_1$. Hence, we obtain

$$\eta_1 = \frac{1}{d_{2\mathrm{D},0}} \int_0^{S_1} \left(1 - \int_{T_{\mathrm{U}}}^{T_{s_1}} \frac{1}{T_{\mathrm{B}} - T_{\mathrm{U}}} \mathrm{d}t \right) \mathrm{d}s_1 = \frac{T_{\mathrm{B}} - T_{\mathrm{U}}}{2\,(T_{\mathrm{F}} - T_{\mathrm{U}})}. \tag{35}$$

Similarly, the mth IRS-UE link will not be blocked when a blockage is horizontally separated from the UE beyond S_2 m in the XOY plane, where

$$S_2 = \frac{T_{\mathrm{B}} - T_{\mathrm{U}}}{h - T_{\mathrm{U}}} d_{2\mathrm{D},m}. \tag{36}$$

Then

$$T_{s_2} = \frac{(h - T_{\mathrm{U}})\, s_2}{d_{2\mathrm{D},m}} + T_{\mathrm{U}} \tag{37}$$

represents the minimum height of a blockage intersecting the IRS-UE link when the blockage is horizontally separated from the UE by s_2 m in the XOY plane, where $0 \le s_2 \le S_2$. Thus, we have

$$\eta_2 = \frac{1}{d_{2\mathrm{D},m}} \int_0^{S_2} \left(1 - \int_{T_{\mathrm{U}}}^{T_{s_2}} \frac{1}{T_{\mathrm{B}} - T_{\mathrm{U}}} \mathrm{d}t \right) \mathrm{d}s_2 = \frac{T_{\mathrm{B}} - T_{\mathrm{U}}}{2\,(h - T_{\mathrm{U}})}. \tag{38}$$

By substituting (31) and (35) into (29) as well as substituting (32) and (38) into (30), (7) and (8) are obtained.

Following [29, Corollary 1], the LoS probability of the mth IRS-UE link is given in (9).

APPENDIX B

The expected value of γ_{Ξ} can be derived following (39) on the next page. For a general case Ξ where $K_{\mathrm{ru},m} \neq 0$, $E\left(|f_{\mathrm{ru},m,n}|\right)$ is a function of d_m. In addition, $E\left[\upsilon^{B_{m,\Xi}}\right]$ or $E\left[\sqrt{\upsilon^{B_{m,\Xi}}}\right]$ is also a function of d_m, as shown in Lemma 1. Hence, if $K_{\mathrm{ru},m} \neq 0$, then $\upsilon^{B_{m,\Xi}}$ and $f_{\mathrm{ru},m,n}$ are not independent to each other.

However, in extremely high blockage density scenarios, (i.e., λ_b is large but finite), all M IRS-UE links are likely to be blocked, making $\Xi = \varnothing$, $\zeta_{\varnothing} \to 1$, $K_{\mathrm{ru},m} \to 0$, and $\mathbf{f}_{\mathrm{ru},m}$ follows Raleigh fading channel, for $m = 1, 2, ..., M$, with $E\left(|f_{\mathrm{ru},m,n}|^2\right) = 1$ and $E\left(|f_{\mathrm{ru},m,n}|\right) = \frac{\sqrt{\pi}}{2}$, which means $E\left(|f_{\mathrm{ru},m,n}|\right)$ is no longer a function of d_m, and is independent of $E\left[\upsilon^{B_m}\right]$ or $E\left[\sqrt{\upsilon^{B_m}}\right]$, resulting in the decoupling of $E\left(\sqrt{\upsilon^{B_m}}|f_{\mathrm{ru},m,n}|\right)$ and $E\left(\upsilon^{B_m}|f_{\mathrm{ru},m,n}|\right)$ [29, Corollary 5.2], thus leading to $\gamma \to E\left(\gamma_{\varnothing}\right)$, the expression after $\overset{(a)}{=}$ in (40).

Moreover, given that

$$\begin{aligned} &E\left[\left(\sum_{n=1}^{N/M} |f_{\mathrm{ru},m,n}|\right)^2\right] \\ &= E\left[\sum_{n_1=1}^{N/M} |f_{\mathrm{ru},m,n_1}|^2 + \sum_{n_1=1}^{N/M} \sum_{\substack{n_2=1,\\ n_2 \neq n_1}}^{N/M} |f_{\mathrm{ru},m,n_1}||f_{\mathrm{ru},m,n_2}|\right] \\ &= \frac{N}{M} + \frac{\pi N}{4M}\left(\frac{N}{M} - 1\right), \end{aligned} \tag{41}$$

$$E\left(|f_{\mathrm{bu}}|^2\right) = 1, E\left(|f_{\mathrm{bu}}|\right) = \frac{\sqrt{\pi}}{2}, \tag{42}$$

$$E\left(\upsilon^{B_m}\right) = \sum_{s=0}^{\infty} \upsilon^s \frac{\left(E\left(B_m\right)\right)^s e^{-E(B_m)}}{s!} = e^{-E(B_m)(1-\upsilon)}, \quad m = 1, 2, .., M, \tag{43}$$

$$\begin{aligned} E\left(\upsilon^{B_0}\right) &= e^{-E(B_0)(1-\upsilon)}, \\ E\left(\sqrt{\upsilon^{B_0}}\right) &= e^{-E(B_0)(1-\sqrt{\upsilon})}, \\ E\left(\sqrt{\upsilon^{B_m}}\right) &= e^{-E(B_m)(1-\sqrt{\upsilon})}, m = 1, 2, ..., M, \end{aligned} \tag{44}$$

by substituting (41-44) into the expression after $\overset{(a)}{=}$ (40), we obtain the expression after $\overset{(b)}{=}$ in (40). By substituting (7), (8), (11) and (5) into the expression after $\overset{(b)}{=}$ in (40), we present $E\left(\gamma_{\varnothing}\right)$ as a function of M, h, λ_{B}, R_{B}, and υ, which is shown in (24).

REFERENCES

[1] Philipp Osterrieder, Lukas Budde, and Thomas Friedli, "The smart factory as a key construct of industry 4.0: A systematic literature review," *International Journal of Production Economics*, vol. 221, no. 107476, Mar. 2020.

[2] B. Chen, *et al.*, "Smart factory of Industry 4.0: key technologies, application case, and challenges," *IEEE Access*, vol. 6, pp. 6505-6519, 2018.

[3] 5G for Connected Industries and Automation. *5G for Connected Industries and Automation*, White Paper (second edition), Feb. 2019.

[4] M. A. Uusitalo et al., "6G vision, value, use cases and technologies from European 6G flagship project Hexa-X," *IEEE Access*, vol. 9, pp. 160004-160020, 2021.

[5] T. M. Ho, *et al.*, "Next-generation wireless solutions for the smart factory, smart vehicles, the smart grid and smart cities,", *arXiv:1907.10102*, Jul. 2019.

[6] A. Anand, G. de Veciana and S. Shakkottai, "Joint scheduling of URLLC and eMBB traffic in 5G wireless networks," *IEEE/ACM Trans. Network.*, vol. 28, no. 2, pp. 477-490, Apr. 2020.

[7] H. Ren, K. Wang and C. Pan, "Intelligent reflecting surface-aided URLLC in a factory automation scenario," *IEEE Trans. Wireless Commun.*, vol. 70, no. 1, pp. 707-723, Jan. 2022.

[8] S. R. Khosravirad, H. Viswanathan and W. Yu, "Exploiting diversity for ultra-reliable and low-latency wireless control," *IEEE Trans. Wireless Commun.*, vol. 20, no. 1, pp. 316-331, Jan. 2021.

[9] G. Ghatak, S. R. Khosravirad and A. De Domenico, "Stochastic geometry framework for ultra-reliable cooperative communications with random blockages," *IEEE Internet of Things Journal*, vol. 9, no. 7, pp. 5150-5161, 1 April, 2022.

[10] M. Alonzo, *et al.*, "URLLC for factory automation: an extensive throughput-reliability analysis of D-MIMO," *24th International ITG Workshop on Smart Antennas*, 2020, pp. 1-6.

[11] B. Singh, *et al.*,, "Ultra-reliable communication in a factory environment for 5G wireless networks: Link level and deployment study," *2016 IEEE 27th Annual International Symposium on Personal, Indoor, and Mobile Radio Communications (PIMRC)*, 2016, pp. 1-5.

[12] X. Mu, *et al.*, "Intelligent reflecting surface enhanced indoor robot path planning: a radio map-based approach," *IEEE Trans. Wireless Commun.*, vol. 20, no. 7, pp. 4732-4747, Jul. 2021.

[13] Z. Liu, Y. Liu and X. Chu, "Reconfigurable-intelligent-surface-assisted indoor millimeter-wave communications for mobile robots," *IEEE Internet of Things Journal*, vol. 11, no. 1, pp. 1548-1557, Jan. 2024.

[14] M. Di Renzo, *et al.*, "Smart radio environments empowered by reconfigurable intelligent surfaces: how it works, state of research, and the road ahead," *IEEE J. Select. Areas Commun.*, vol. 38, no. 11, pp. 2450-2525, Nov. 2020.

[15] Y. Guan, , *et al.*, "A comparative study for indoor factory environments at 4.9 and 28 GHz," *2020 14th European Conference on Antennas and Propagation (EuCAP)*, 2020, pp. 1-5.

[16] D. Chizhik, *et al.*, "Path loss and directional gain measurements at 28 GHz for factory automation" *2019 IEEE International Symposium on Antennas and Propagation and USNC-URSI Radio Science Meeting*, 2019, pp. 2143-2144.

[17] D. Solomitckii, *et al.*, "Characterization of mmWave channel properties at 28 and 60 GHz in factory automation deployments," *2018 IEEE Wireless Communications and Networking Conference (WCNC)*, 2018, pp. 1-6.

[18] T. Jiang, *et al.*, "3GPP standardized 5G channel model for IIoT scenarios: a survey," *IEEE Internet of Things Journal*, vol. 8, no. 11, pp. 8799-8815, Jun. 2021.

[19] A. Papazafeiropoulos, *et al.*, "Coverage probability of distributed IRS systems under spatially correlated channels," *IEEE Wireless Commun. Lett.*, vol. 10, no. 8, pp. 1722-1726, Aug. 2021.

[20] Z. Zhang, *et al.*, "Analysis and optimization of outage probability in

$$
\begin{aligned}
E\left(\gamma_{\Xi}\right) &= \rho E\left(\left(\sqrt{\beta_0\omega\upsilon^{B_0}}\left|f_{\mathrm{bu}}\right|+\sum_{m=1}^{M}\sqrt{\beta_m\upsilon^{B_{m,\Xi}}}\sum_{n=1}^{N/M}\left|f_{\mathrm{ru},m,n}\right|\right)^2\right) \\
&= \rho\left(\begin{array}{l}
\beta_0\omega E\left[\upsilon^{B_0}\left|f_{\mathrm{bu}}\right|^2\right]+2\sqrt{\beta_0\omega}\sum\limits_{m=1}^{M}\sqrt{\beta_m}E\left[\sqrt{\upsilon^{(B_0+B_{m,\Xi})}}\left|f_{\mathrm{bu}}\right|\sum\limits_{n=1}^{N/M}\left|f_{\mathrm{ru},m,n}\right|\right] \\
+\sum\limits_{m=1}^{M}\sum\limits_{p=1,p\neq m}^{M}\sqrt{\beta_m\beta_p}E\left[\sqrt{\upsilon^{(B_{p,\Xi}+B_{m,\Xi})}}\sum\limits_{n_1=1}^{N/M}\left|f_{\mathrm{ru},p,n_1}\right|\sum\limits_{n_2=1}^{N/M}\left|f_{\mathrm{ru},m,n_2}\right|\right] \\
+\sum\limits_{m=1}^{M}\beta_m E\left[\upsilon^{B_{m,\Xi}}\left(\sum\limits_{n=1}^{N/M}\left|f_{\mathrm{ru},m,n}\right|\right)^2\right]
\end{array}\right)
\end{aligned} \tag{39}
$$

$$
\begin{aligned}
E\left(\gamma_{\varnothing}\right) &\overset{(a)}{=} \rho\left(\begin{array}{l}
\beta_0\omega E\left[\upsilon^{B_0}\right]E\left[\left|f_{\mathrm{bu}}\right|^2\right] \\
+2\sqrt{\beta_0\omega}\sum\limits_{m=1}^{M}\sqrt{\beta_m}E\left[\sqrt{\upsilon^{(B_0+B_m)}}\right]E\left[\sum\limits_{n=1}^{N/M}\left|f_{\mathrm{bu}}\right|\left|f_{\mathrm{ru},m,n}\right|\right] \\
+\sum\limits_{m=1}^{M}\sum\limits_{p=1,p\neq m}^{M}\sqrt{\beta_m\beta_p}E\left[\sqrt{\upsilon^{(B_p+B_m)}}\right]E\left[\sum\limits_{n_1=1}^{N/M}\left|f_{\mathrm{ru},p,n_1}\right|\sum\limits_{n_2=1}^{N/M}\left|f_{\mathrm{ru},m,n_2}\right|\right] \\
+\sum\limits_{m=1}^{M}\beta_m E\left[\upsilon^{B_m}\right]E\left[\left(\sum\limits_{n=1}^{N/M}\left|f_{\mathrm{ru},m,n}\right|\right)^2\right]
\end{array}\right) \\
&\overset{(b)}{=} \rho\left(\begin{array}{l}
\beta_0\omega\exp\left(-E\left(B_0\right)\left(1-v\right)\right) \\
+\sqrt{\beta_0\omega}\frac{\pi N}{2M}\sum\limits_{m=1}^{M}\sqrt{\beta_m}\exp\left(-\left(E\left(B_0\right)+E\left(B_m\right)\right)\left(1-\sqrt{v}\right)\right) \\
+\frac{\pi N^2}{4M^2}\sum\limits_{m=1}^{M}\sum\limits_{p=1,p\neq m}^{M}\sqrt{\beta_m\beta_p}\exp\left(-\left(E\left(B_p\right)+E\left(B_m\right)\right)\left(1-\sqrt{v}\right)\right) \\
+\left(\frac{N}{M}+\frac{N}{M}\left(\frac{N}{M}-1\right)\frac{\pi}{4}\right)\sum\limits_{m=1}^{M}\beta_m\exp\left(-E\left(B_m\right)\left(1-v\right)\right)
\end{array}\right)
\end{aligned} \tag{40}
$$

multi-intelligent reflecting surface-assisted systems," *arXiv: 1909.02193*, Sep. 2019.
[21] D. L. Galappaththige, D. Kudathanthirige and G. Amarasuriya, "Performance analysis of distributed intelligent reflective surface aided communications," *2020 IEEE Global Communications Conference*, 2020, pp. 1-6.
[22] Y. Gao, *et al.*, "Distributed IRS with statistical passive beamforming for MISO communications," *IEEE Wireless Commun. Lett.*, vol. 10, no. 2, pp. 221-225, Feb. 2021.
[23] J. Lyu and R. Zhang, "Spatial throughput characterization for intelligent reflecting surface aided multiuser system," *IEEE Wireless Commun. Lett.*, vol. 9, no. 6, pp. 834-838, Jun. 2020.
[24] J. Ye, A. Kammoun and M. -S. Alouini, "Spatially-distributed RISs vs relay-assisted systems: a fair comparison," *IEEE Open Journal of the Communications Society*, vol. 2, pp. 799-817, 2021.
[25] M. A. Kishk and M. S. Alouini, "Exploiting randomly located blockages for large-scale deployment of intelligent surfaces," *IEEE J. Select. Areas Commun.*, vol. 39, no. 4, pp. 1043-1056, Apr. 2021.
[26] Z. Li, *et al.*, "RIS-assisted mmWave networks with random blockages: fewer large RISs or more small RISs?," *IEEE Trans. Wireless Commun.*, 2022, early access.
[27] H. Ren, C. Pan and K. Wang, "Average data rate and decoding error probability analysis for IRS-aided URLLC in a factory automation scenario," *2021 IEEE/CIC International Conference on Communications in China (ICCC Workshops)*, 2021, pp. 177-182.
[28] N. Rubab, *et al.*, "Interference mitigation in RIS-assisted 6G systems for indoor industrial IoT networks," *2022 IEEE 12th Sensor Array and Multichannel Signal Processing Workshop (SAM)*, 2022, pp. 211-215.
[29] T. Bai, R. Vaze and R. W. Heath, "Analysis of blockage effects on urban cellular networks," *IEEE Trans. Wireless Commun.*, vol. 13, no. 9, pp. 5070-5083, Sep. 2014.
[30] W. Mei and R. Zhang, "Multi-beam multi-hop routing for intelligent reflecting surfaces aided massive MIMO," *IEEE Trans. Wireless Commun.*, vol. 21, no. 3, pp. 1897-1912, Mar. 2022.
[31] T. N. Do, *et al.*, "Multi-RIS-aided wireless systems: statistical characterization and performance analysis," *IEEE Trans. Commun.*, vol. 69, no. 12, pp. 8641-8658, Dec. 2021.
[32] E. Björnson and L. Sanguinetti, "Rayleigh fading modeling and channel hardening for reconfigurable intelligent surfaces," *IEEE Wireless Commun. Lett.*, vol. 10, no. 4, pp. 830-834, Apr. 2021.
[33] 3rd Generation Partnership Project, "Study on channel model for frequencies from 0.5 to 100 GHz (3GPP TR 38.901 version 16.1.0 Release 16)," Dec. 2019.
[34] W. Tang, *et al.*, "Wireless communications with reconfigurable intelligent surface: path loss modeling and experimental measurement," *IEEE Trans. Wireless Commun.*, vol. 20, no. 1, pp. 421-439, Jan. 2021.
[35] P. Wang, *et al.*, "Intelligent reflecting surface-assisted millimeter wave communications: joint active and passive precoding design," *IEEE Trans. Veh. Technol.*, vol. 69, no. 12, pp. 14960-14973, Dec. 2020.
[36] *Communication Receivers*, U Rohde & T Bucher, 1998, McGraw Hill.
[37] Y. Polyanskiy, H. V. Poor and S. Verdu, "Channel coding rate in the finite blocklength regime," *IEEE Trans. Inform. Theory*, vol. 56, no. 5, pp. 2307-2359, May 2010.
[38] F. Alsaleem, J. S. Thompson, D. I. Laurenson, C. A. Alistarh and S. K. Podilchak, "Small-size blockage propagation modeling at 28 GHz for mmWave communications systems," *IEEE Trans. Antenna Propagat.*, vol. 70, no. 9, pp. 8578-8583, Sept. 2022.

Yixin Zhang (Member, IEEE) received the B.Eng. degree in electronic and information engineering from the Beijing University of Posts and Telecommunications (BUPT), Beijing, China, in 2017, and the Ph.D. degree in electronic and electrical engineering from The University of Sheffield, Sheffield, U.K., in 2022. She was with Nokia Bell Labs, Espoo, Finland, from 2020 to 2022, and Televic Conference, Izegem, Belgium, from 2019 to 2020. She is currently a Lecturer with the School of Information and Communication Engineering, BUPT. Her research interests include the smart built environment, intelligent reflective surface, electromagnetic wave propagation, channel characterization, and MIMO antenna configuration. Dr. Zhang was awarded a Marie Sklodowska-Curie Fellowship in 2018.

Saeed R. Khosravirad (Senior Member, IEEE) is a Member of Technical Staff at Nokia Bell Labs, NJ, USA. He received his Ph.D. degree in telecommunications in 2015 from McGill University, Canada. Prior to that, he received the B.Sc. degree from the department of Electrical and Computer Engineering, University of Tehran, Iran, and the M.Sc. degree from the department of Electrical Engineering, Sharif University of Technology, Iran. During 2018-2019, he was with the Electrical & Computer Engineering department of University of Toronto, Canada as a Visiting Scholar. He is a co-editor of the book Ultra-Reliable and Low-Latency Communications (URLLC) Theory and Practice: Advances in 5G and Beyond (Wiley 2023), editor of the IEEE Transactions on Wireless Communications, editor of the IEEE Communications Magazine, and guest editor of the IEEE Wireless Communications magazine. He is interested in interdisciplinary research, understanding the interworking between wireless communications theory, control theory, artificial intelligence, and circuit theory.

Xiaoli Chu (Senior Member, IEEE) received the B.Eng. degree in electronic and information engineering from Xi'an Jiaotong University, Xi'an, China, in 2001, and the Ph.D. degree in electrical and electronic engineering from The Hong Kong University of Science and Technology, Hong Kong, in 2005. From 2005 to 2012, she was with the Centre for Telecommunications Research, King's College London, London, U.K. She is currently a Professor with the Department of Electronic and Electrical Engineering, The University of Sheffield, Sheffield, U.K. She has co-authored over 200 peer-reviewed journals and conference papers, including eight ESI Highly Cited Papers and the IEEE Communications Society 2017 Young Author Best Paper. She co-authored/co-edited the books Fog-Enabled Intelligent IoT Systems (Springer 2020), Ultra Dense Networks for 5G and Beyond (Wiley 2019), Heterogeneous Cellular Networks-Theory, Simulation and Deployment (Cambridge University Press 2013), and 4G Femtocells: Resource Allocation and Interference Management (Springer 2013). Dr. Chu received the IEEE COMMUNICATIONS LETTERS Exemplary Editor Award in 2018. She is a Senior Editor of IEEE WIRELESS COMMUNICATIONS LETTERS and an Associate Editor of IEEE TRANSACTIONS ON NETWORK SCIENCE AND ENGINEERING, IEEE OPEN JOURNAL OF VEHICULAR TECHNOLOGY, and IEEE TRANSACTIONS ON MACHINE LEARNING IN COMMUNICATIONS AND NETWORKING.

Mikko A. Uusitalo (Senior Member, IEEE) is Head of Research Department Radio Systems Research Finland at Nokia Bell Labs. Mikko is leading the European 6G Flagship project Hexa-X-II and was leading Hexa-X. He obtained a M.Sc. (Eng.) and Dr.Tech. in 1993 and 1997 and a B.Sc. (Economics) in 2003, all from predecessors of Aalto University. Mikko has been at Nokia since 2000 with various roles, including Principal Researcher and Head of International Cooperation at Nokia Research. Mikko is a founding member of the CELTIC EUREKA and WWRF, the latter one he chaired for 2004-2006. Mikko is a WWRF Fellow. Mikko has been nominated among Nokia top inventors six times, Mikko's H-index is 40+ and i10-index 100+. Mikko has more than 230 granted patents. In 2020 Mikko received the Cross of Merit of the Order of White Rose from the President of Finland. Mikko has and has had numerous board and advisory positions in many important groups in the industry, academia or government side.